Co-published by
Institute of Fluid-Flow Machinery
Polish Academy of Sciences
Committee on Thermodynamics and Combustion
Polish Academy of Sciences

Copyright©2024 by the Authors under licence CC BY 4.0

http://www.imp.gda.pl/archives-of-thermodynamics/

ARCHIVES OF THERMODYNAMICS

Asymmetrical melting and solidification processes of phase change material and the challenges for thermal energy storage systems

Inge Magdalena Sutjahja[a*], Akhmad Yusuf[a], Yunita Anggraini[a], Shofi Dhiya Ulhaq[a], Daniel Kurnia[a], Surjamanto Wonorahardjo[b]

[a] Physics Department, FMIPA, Institut Teknologi Bandung, Jl. Ganesha No. 10, Bandung 40132, Indonesia
[b]Building Technology Research Group, SAPPK, Institut Teknologi Bandung, Jl. Ganesha No. 10, Bandung 40132, Indonesia
*Corresponding author email: im_sutjahja@itb.ac.id

Received: 23.12.2023; revised: 10.05.2024; accepted: 28.05.2024

Abstract

The melting and solidification processes of the organic phase change material – lauric acid exposed to air were experimentally studied to investigate the heat exchange and its effect on the heat transfer behaviour inside a shell as well as its phase-change characteristics. Lauric acid was placed in spherical shells made of polyvinyl chloride with diameters of 44, 63, and 74 mm. This study was based on analyses of the surface temperature and vertical temperature distribution data inside the shells. We found that the phase change characteristics were strongly related to the dominant heat transfer mechanism. In this case, melting was dominated by convection, whereas solidification was dominated by conduction. The convection intensity increased as the shell diameter increased. Further analysis revealed the melting and solidification periods. In contrast to latent heat release accompanying solidification, latent heat absorption accompanied by melting does not occur at a constant temperature, although it has a smaller temperature gradient than does sensible heat absorption. Based on the asymmetry between the melting and solidification processes, we discuss various possible strategies by which to control the charging and discharging of the phase change material by restraining the heat transfer rate to optimise its performance as a latent thermal energy storage material.

Keywords: Phase change material; Lauric acid; Heat transfer rate; Asymmetry melting and solidification; Heat transfer control

Vol. 45(2024), No. 1, 135–147; doi: 10.24425/ather.2024.151224

Cite this manuscript as: Sutjahja, I.M., Yusuf, A., Anggraini, Y., Ulhaq, S.D., Kurnia, D., & Wonorahardjo, S. (2024). Asymmetrical melting and solidification processes of phase change material and the challenges for thermal energy storage systems. *Archives of Thermodynamics*, 45(3), 135−147.

1. Introduction

Organic phase-change materials (PCMs) for latent thermal energy storage (TES) have emerged as suitable materials for storing and releasing large amounts of energy at relatively constant temperatures during the solid-to-liquid phase transition, or vice versa [1,2]. Organic PCMs have several attractive features such as congruent melting, high latent heat of fusion, nontoxicity, nonflammability, little or no volume change, extremely small or even negligible supercooling, low cost, high thermal stability, good chemical stability over many thermal cycles, compatibility with several types of container materials, and environmental and human friendliness [3–7]. Among the organic PCMs, saturated

Nomenclature

A – heat transfer area, m^2
h – convective heat transfer coefficient, W/(m^{2}K)
L – length, m
P – power density, W/m^2
$\dot{Q}$ – rate of heat, W
t_f – beginning of freezing time, min
t_{if} – end of the solidification, min
t_m – beginning of melting time, min
t_{pm} – end of melting time, min
T_b – temperature at half-bottom, inside the sample, °C
T_c – temperature at centre, inside the sample, °C
T_f – freezing temperature, °C
T_m – melting temperature, °C
$T_{s,b}$ – temperature at bottom surface, °C
$T_{s,u}$ – temperature at upper surface, °C
T_u – temperature at half-upper, inside the sample, °C

Greek symbols

Δt_c – solidification period, min
Δt_m – melting period, min
κ – thermal conductivity, W/(m K)

Subscripts

a – ambient
c – container
w – boundary

Abbreviations and Acronyms

LA – lauric acid
HTF – heat transfer fluid
PCM – phase change material
TES – thermal energy storage

fatty acids with the general formula $CH_3(CH_2)_nCOOH$ are of particular interest because the melting temperature of a material is proportional to the number of carbon atoms, that is the chemical bond between carbon and hydrogen. Therefore, this material can be easily selected for certain applications. Fatty acids have been used in several fields including building components [8–10], solar energy storage applications [6], temperature-regulated drug-delivery systems [11], and biological applications [12].

For energy storage applications in buildings, the macroencapsulation of organic PCMs is beneficial because of their simplicity and relatively low cost [13–15]. It is implemented as either an internal thermal mass [16,17] or a building envelope [13,15] to reduce building energy consumption, reduce the cooling load, achieve room cooling, and improve indoor thermal comfort. Focusing on the spherical geometry, which exhibits the highest thermal performance [18], the heat transfer rate of PCMs in spherical cells can be easily adjusted from the surface-area-to-volume ratio [19]. In practical applications, the common phase change of PCM is solid-to-liquid (melting) or vice versa (solidification). The melting and solidification processes of PCM involve conduction and convection heat transfers, each with different characteristics and heat transfer rates [20]. In addition, depending on the effects of gravitation on the solid phase of the PCM, the melting process can follow one of two possible mechanisms: constrained or unconstrained. In constrained melting, the solid PCM is prevented from sinking to the bottom of the sphere using a glass-enclosed thermocouple, whereas in unconstrained melting, the solid PCM sinks to the bottom of the sphere owing to gravity [21]. The melting rate is slower in constrained fusion than in unconstrained fusion [21,22].

Numerous theoretical, simulation and experimental studies have been performed to study the melting and solidification of PCMs in a spherical geometry, as summarised in Table 1, which outlines the surrounding fluid as the heat transfer fluid (HTF) as well as the output parameters from the study. In addition to the temperature difference and surface area, the properties of the fluid, nature of the fluid motion, and bulk fluid velocity are variables that determine the convection heat transfer coefficient for the heat exchange rate between the PCM and the environment as well as the heat transfer rate inside the PCM. The higher the density of the fluid and faster the fluid motion, the greater the convective heat transfer [20]. As shown in Table 1, water is commonly used as the fluid; however, for various applications, PCM can be used with different types of HTF, including air [23,24]. Because of the relatively high density, viscosity and thermal conductivity of water compared with air, a steady state can be achieved in a relatively short time, after which the surface temperature of the PCM can be assumed constant. This condition allows for a comparison between the results of the experimental and simulation studies, with the time evolution of the liquid or solid fraction as a common comparative output parameter. The results of the experimental and simulation studies show that during a solid-to-liquid phase change using water at a constant temperature or water with variable electrical power [25], the temperature inside the PCM increases sharply around the melting point [21,26–28]. This contrasts with the liquid-to-solid phase change that occurs at relatively constant temperature [29]. For melting and solidification with forced air convection [30], a high transfer rate obliterates the phase change characteristics at a constant temperature. The drastic change in the PCM temperature during the phase transition raises the question of its capability as a latent TES that can absorb and release a relatively large amount of thermal energy at a constant temperature.

In this study, the melting and solidification processes of an organic PCM of lauric acid (LA) encapsulated in a spherical shell exposed to a natural air environment were experimentally studied to investigate the relationship between the dominant heat transfer and heat transfer rate, and its implication on the phase change characteristics for its application as latent thermal energy storage. The use of air instead of water as the medium for the phase change of LA allowed us to study the heat exchange process in detail owing to the slower heat transfer rate. Based on the asymmetry between the melting and solidification processes, we discuss several possible methods for controlling the heat transfer rate to optimise the performance of a PCM as a latent TES.

Table 1. Phase change studies of PCMs contained in a spherical enclosure with environmental conditions and output parameters.

Author/Ref.	Process		Method		HTF/Environment condition	Output parameter
	Melting	Solidification	Theory/simulation	Experiment		
Tan, 2008 [21]	√			√	Water bath with constant temperatures	Melting phase front, liquid fraction, time dependent temperature
Kothari et al., 2020 [22]	√		√		A constant wall temperature	Melt fraction
Rizan et al., 2012 [25]	√			√	Water bath with constant heat rates at surface	Phase front and isotherm, melt-fraction, Stefan number
Galione et al., 2015 [26]	√	√	√		Water bath at a constant temperature	Time dependent temperature, liquid fraction, temperature map
Hosseinizadeh et al., 2013 [27]	√		√	√	Constant wall temperatures	Melt fraction, melting phase front, temperature contour and streamline, heat flux, time dependent temperature, Nusselt number
Tan et al., 2009 [28]	√		√	√	Constant surface wall temperature	Melt fraction, streamline, temperature contour, time dependent temperature
Ismail and Moraes, 2009 [29]		√	√	√	Constant surface temperatures	Time dependent temperature, solidified mass fraction
Ettouney et al., (2005) [30]	√	√		√	Air at constant temperatures and different velocities.	Time dependent temperature, Nusselt number, Fourier number
Toledo et al., 2022 [31]	√	√	√		Water bath at constant temperatures	Liquid fraction, heat flow, Nusselt number
Assis et al., 2007 [32]	√		√	√	Constant wall temperatures	Melt fraction, heat flux
Li et al., 2017 [33]	√		√		Water bath at constant temperatures	Melt fraction
Ghosh et al., 2019 [34]		√	√		Constant surface temperature	Melt fraction, heat flux
Nazzi Ehms et al., 2018 [35]		√	√		Constant surface temperatures	Solid/liquid fraction, heat flux, streamline, temperature line, heat flux
Assis et al., 2009 [36]		√	√	√	Uniform wall temperatures	Melt fraction
Li et al., 2015 [37]	√	√		√	Water bath with a constant temperature	Time dependent temperature
Prabakaran et al., 2020 [38]	√			√	Constant temperature bath of water	Time dependent temperature

2. Materials and methods

We use technical LA with a purity of ≥ 98%. The thermophysical parameters of LA are listed in Table 2.

Table 2. Thermophysical parameters of LA from the previous experimental studies (*s*: solid, *l*: liquid).

Thermophysical parameters	Value	Ref.
Melting temperature, °C	45	[39]
Freezing temperature, °C	41	[39]
Latent heat, kJ/kg	187	[39]
Density, kg/m^3	940 (*s*), 885 (*l*)	[40]
Specific heat, kJ/kg °C	2.18 (*s*), 2.39 (*l*)	[40]
Thermal conductivity, W/m °C	0.169 (*s*), 0.144 (*l*)	[39]
Viscosity, kg/m s	3.74 (55 °C) 4.565 (70 °C) 6.325 (80 °C)	[39]

Figure 1 shows the experimental setup used to study the melting and solidification of LA in air. Three spherical shells with outer diameters of 44 mm, 63 mm, and 74 mm were filled with LA. We used commercial spherical shells, which were made of polyvinyl chloride with a thickness of approximately 0.5 mm. The mass of the sample inserted into the sphere was reduced by approximately 1% of its maximum value, allowing volume expansion during phase transition. The melting process was performed in a cubical adiabatic bath that could be set to a maximum temperature of 87°C, provided by four heating elements connected to a voltage controller and a step-down transformer for temperature setting. For homogeneous temperature distribution, the heating elements were covered with ceramic and glass wool and placed at the bottom of the room. The ceramic acts as a thermal mass that stabilises the temperature when the PCM shell is inserted. The maximum difference in the temperature along the vertical configuration is approximately 1°C.

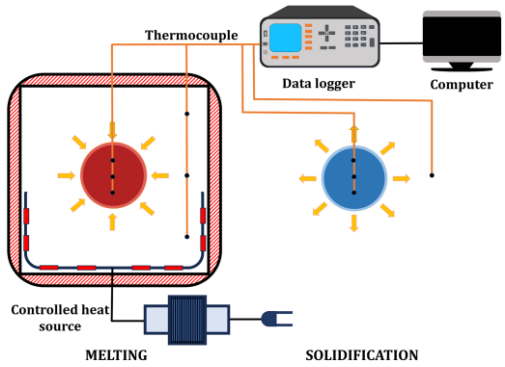

Fig. 1. Experimental setup for melting and solidification LA in air environment.

The temperature sensor consists of a T-type thermocouple with an accuracy of 0.2% + 1°C and is part of a multichannel data logger. Temperature data were recorded at time intervals of 5 s. For each spherical LA, three temperature sensors tied to a stick were placed vertically inside the shell, and two temperature sensors were placed at the upper and lower parts of the outer surface of the shell, as shown in Fig. 2. The positions of the temperature sensors and their symbols are listed in Table 3.

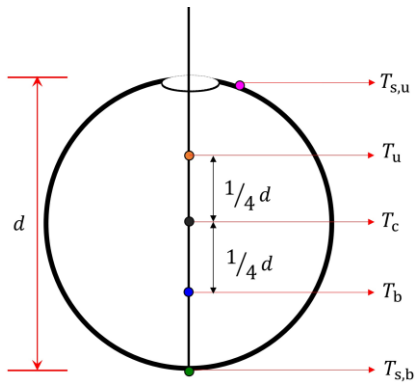

Fig. 2. Sensor position and symbol.

Table 3. Position of temperature sensors and its symbols.

Position	Symbol
Upper surface	$T_{s,u}$
Half-upper, inside the sample	T_u
Centre, inside the sample	T_c
Half-bottom, inside the sample	T_b
Bottom surface	$T_{s,b}$

For the melting process, the solid LA at room temperature (25°C) was exposed to an 80°C environment in an adiabatic room. However, for the solidification process, the melted LA at 80°C was cooled to room temperature in a natural air environment at 25°C. For each process, the experiment was repeated thrice to ensure data repeatability.

3. Results and discussion

3.1. The heat absorption associated with the melting process of lauric acid

Figure 3(i) illustrates the temperature versus time for the melting process of LA in a spherical shell with a diameter of 44 mm for the sensors on the upper (T_u), centre (T_c), and bottom (T_b) of the shell, along with the surface temperature data for $T_{s,u}$ and $T_{s,b}$. In addition to the LA temperature, the temperature data of T_u were influenced by the opening at the top of the shell. Hence, the small opening acts as a medium for convection in air. Furthermore, both surface temperatures were affected by the outside air temperature and the LA temperature inside the shell.

Starting from a room temperature of approximately 25°C, the melting process of LA involves the absorption of sensible heat in the solid phase with a significant temperature change up to the melting temperature (T_m), followed by latent heat absorption from the solid-to-liquid phase change process at T_m and subsequent sensible heat absorption in the liquid phase. Heat absorption in the sensible and latent phases is indicated by temperature changes, although the solid-to-liquid phase transition occurs with a smaller temperature gradient than that in the sensible phase. Latent heat absorption at a relatively constant temperature occurred only for the sensor at the bottom (T_b). This result is in agreement with those of previous experimental studies on the melting of PCM using a water bath with a relatively small temperature gradient [37,38].

The dominance of the convection heat transfer mode during the melting process was indicated by the different temperature profiles inside and on the surface of the shell. Because of air convection outside the shell, T_{su} was always higher than T_{sb}, except at the beginning and end of the process, when equilibrium occurred. The skin of the shell provided thermal resistance between the outside air and the PCM inside the shell such that T_u was lower than T_{su} and T_b was lower than T_{sb}. The temperature differences ($T_{s,u}$–T_c) and ($T_{s,b}$–T_c) (Fig. 3(ii)) are proportional to the heat exchanged between the PCM and the environment. Anisotropic heat exchange characteristics were observed for the upper and lower surfaces of the shell; however, they decreased as they approached thermal equilibrium. A large heat exchange occurred during the solid-to-liquid phase transition (see Section 3.3 for the analysis, as indicated by the dotted and dashed lines in Figs. 3(i) and 3(ii)). Concerning the melting mechanism, constrained melting occurs from the beginning up to a certain time, depending on the shell diameter, as indicated by $T_b < T_{sb}$. As time increases, the solid part of the LA collapses; therefore, $T_b > T_{sb}$, and constrained melting was replaced by unconstrained melting. For various shell diameters, a transition from constrained to unconstrained melting occurred at approximately 70 min for 44 mm, 108 min for 63 mm, and 130 min for 74 mm, as indicated by the valley in (T_{sb}–T_c) in Fig. 3(ii).

To study the heat transfer inside the shell during melting, Fig. 4 shows the temperature distribution along the vertical direction at certain times. From this heat absorption profile, we observed that inside the PCM shell, the melting process started from the upper part to the bottom, such that $T_u > T_c > T_b$ for all measurements. This result suggests that the phase transition process at the upper part is the fastest, followed by that at the centre and bottom parts of the shell, because of the sinking of the solid phase to the bottom owing to its higher density. From the heat conduction mode in the solid phase, heat transfer was converted into heat convection, as signified by the asymmetric temperature profiles inside the shell and the large temperature difference or gap in the temperature distribution. The convection at the upper part of the shell was stronger than that at the centre and bottom.

From the beginning (left panel of Fig. 4) to the end of the melting process (right panel of Fig. 4), the temperature distribution shown in Fig. 4 clearly indicated a larger convection with increasing shell diameter. This was also clarified by the difference between T_u and T_b with respect to dimensionless time, which was defined as the absolute time divided by the shell radii, as shown in Fig. 5. As the shell diameter increases, the (T_u–T_b) values increase, implying a higher convection intensity [30]. In

addition, for each shell, the temperature difference of (T_u–T_b) showed double peaks, with a smaller peak after the beginning of the melting time and a larger peak before the end of the melting time (see Section 3.3 for the analysis of the melting period).

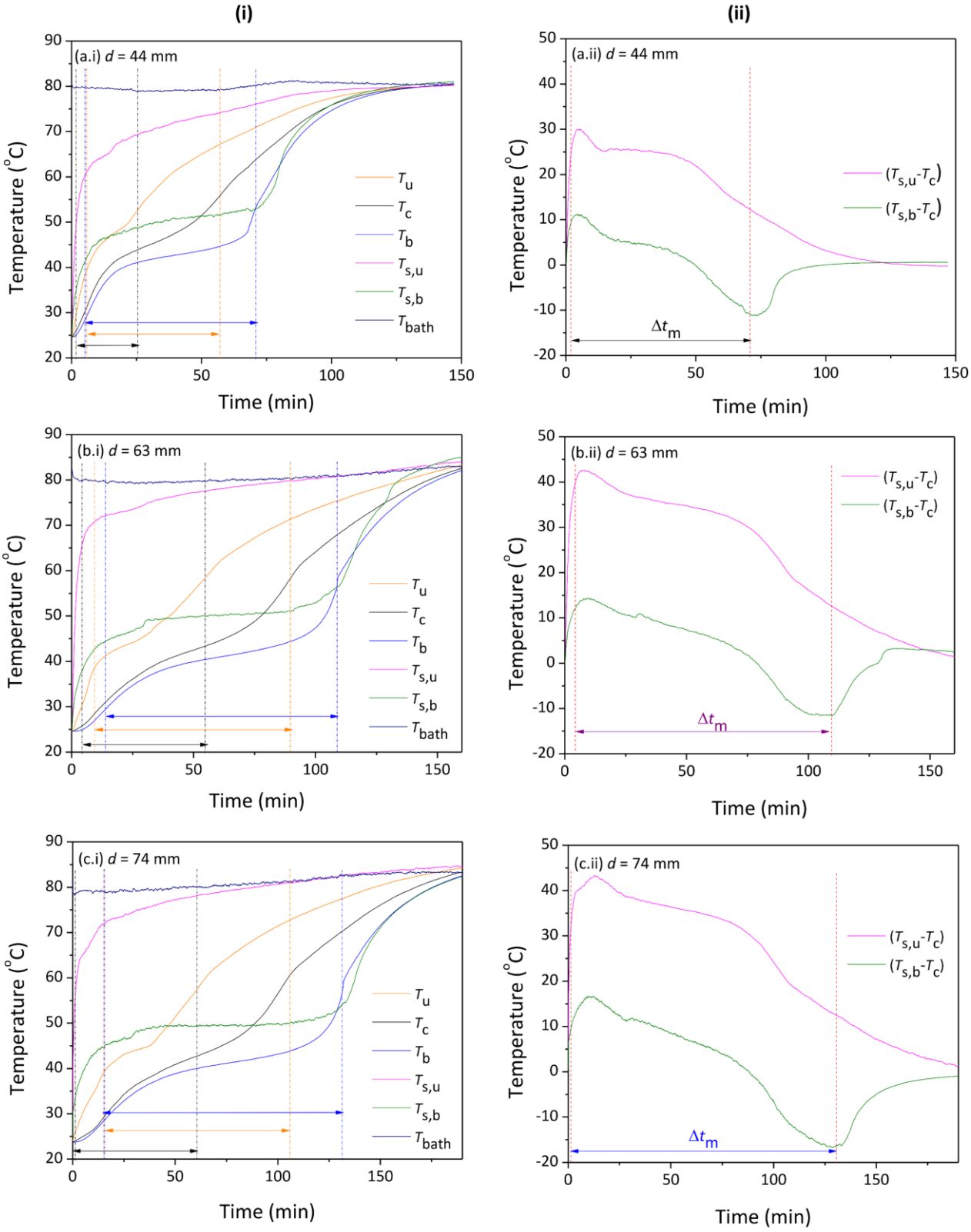

Fig. 3. Experimental data of the melting of LA in a spherical shell with outer diameters of (a) 44 mm, (b) 63 mm, and (c) 74 mm. Left (i): temperature data inside the sample (T_u, T_c, and T_b), surface temperature data ($T_{s,u}$ and $T_{s,b}$), and bath temperature (T_{bath}). Vertical dotted lines denote the phase transition region for each sensor inside the shell. Right (ii): the temperature differences of ($T_{s,u}$–T_c) and ($T_{s,b}$–T_c) with vertical dashed lines denote the melting period.

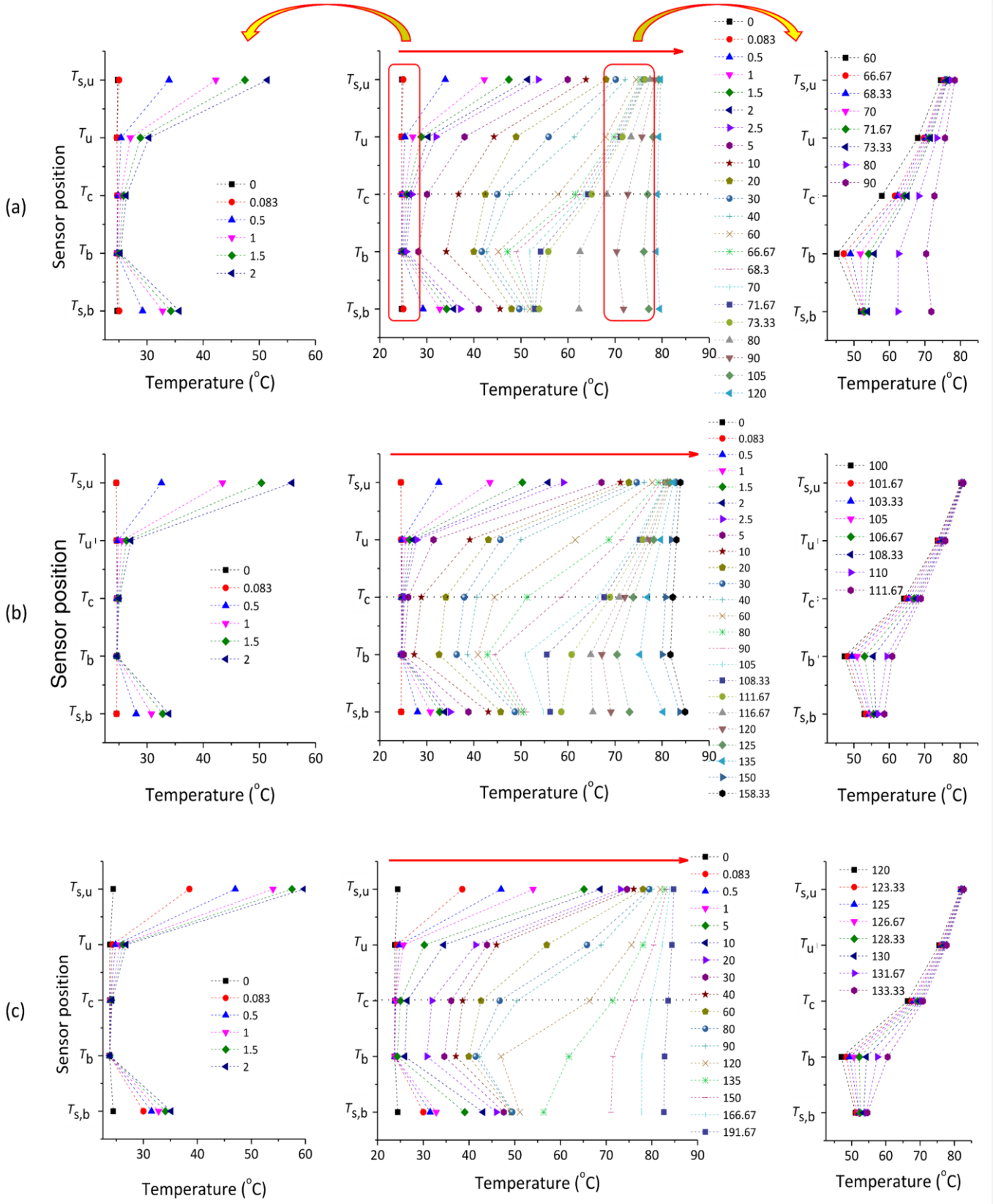

Fig. 4. Temperature distribution along the vertical direction at certain times (in minute) during melting of LA in a spherical shell with diameters of (a) 44 mm, (b) 63 mm, and (c) 74 mm (the arrow indicates the process direction). Middle column: overall time range, left column: beginning of process, right column: near end process.

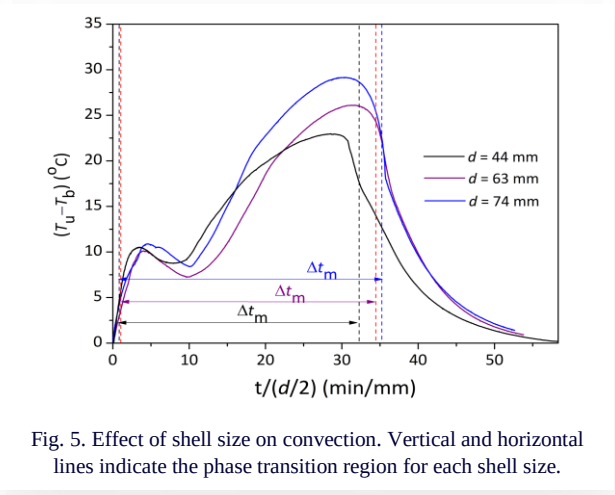

Fig. 5. Effect of shell size on convection. Vertical and horizontal lines indicate the phase transition region for each shell size.

3.2. The heat release associated with the solidification process of lauric acid

From the time-dependent temperature during the solidification process (Fig. 6(i)), we observed that starting from a high temperature of approximately 80°C, the solidification process of LA involved the release of sensible heat in the liquid phase with a significant temperature change up to the freezing temperature (T_f), followed by latent heat release from the liquid-to-solid phase change process at T_f and the subsequent sensible heat release in the solid phase. No significant differences were observed in the temperature data at the centre and bottom of the sample. Furthermore, the liquid-to-solid phase transition occurred at a relatively constant temperature of 43°C, and no supercooling was observed in the freezing curve.

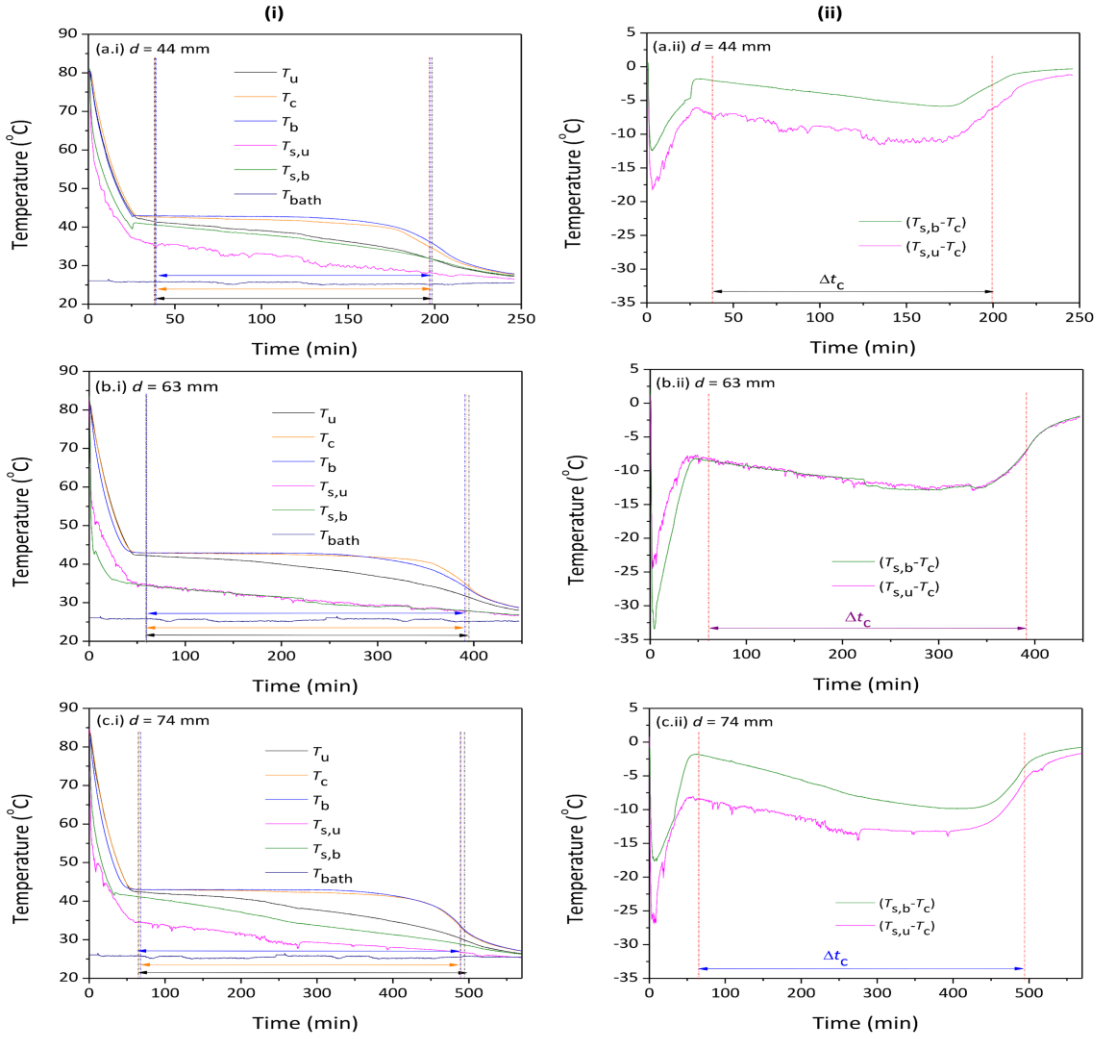

Fig. 6. Time-dependent temperature data during the solidification of LA in a spherical shell with outer diameters of (a) 44 mm, (b) 63 mm, and (c) 74 mm. Left (i): temperature data inside the sample (T_u, T_c, and T_b), surface temperature data ($T_{s,u}$ and $T_{s,b}$), and bath temperature (T_{bath}). Vertical dotted lines denote the phase transition region for each sensor inside the shell. Right (ii): the temperature differences of ($T_{s,u}$–T_c) and ($T_{s,b}$–T_c) with vertical dashed lines denote the solidification period.

Compared with melting, the isotropic heat exchange over the surface of the shell is shown in Fig. 6 (ii) which shows a similarity in the temperature differences of ($T_{s,u}$–T_c) and ($T_{s,b}$–T_c).

The temperature distributions at certain times during solidification are shown in Fig. 7. Initially, the temperature distribution inside the shell was relatively homogenous, and the surface

temperature was lower than that inside the shell owing to the influence of the environment. With increasing time, the temperature distribution inside the shell became inhomogeneous, and a gap in the temperature distribution was observed. Because of convection, T_c was always higher than T_u and T_u was higher than T_b. The gap in the temperature distribution diminished after a certain time, that is approximately 30, 40 and 60 minutes for shell diameters of 44, 63 and 74 mm, respectively. Hence, the heat transfer mechanism may change from convection to conduction following the phase change process.

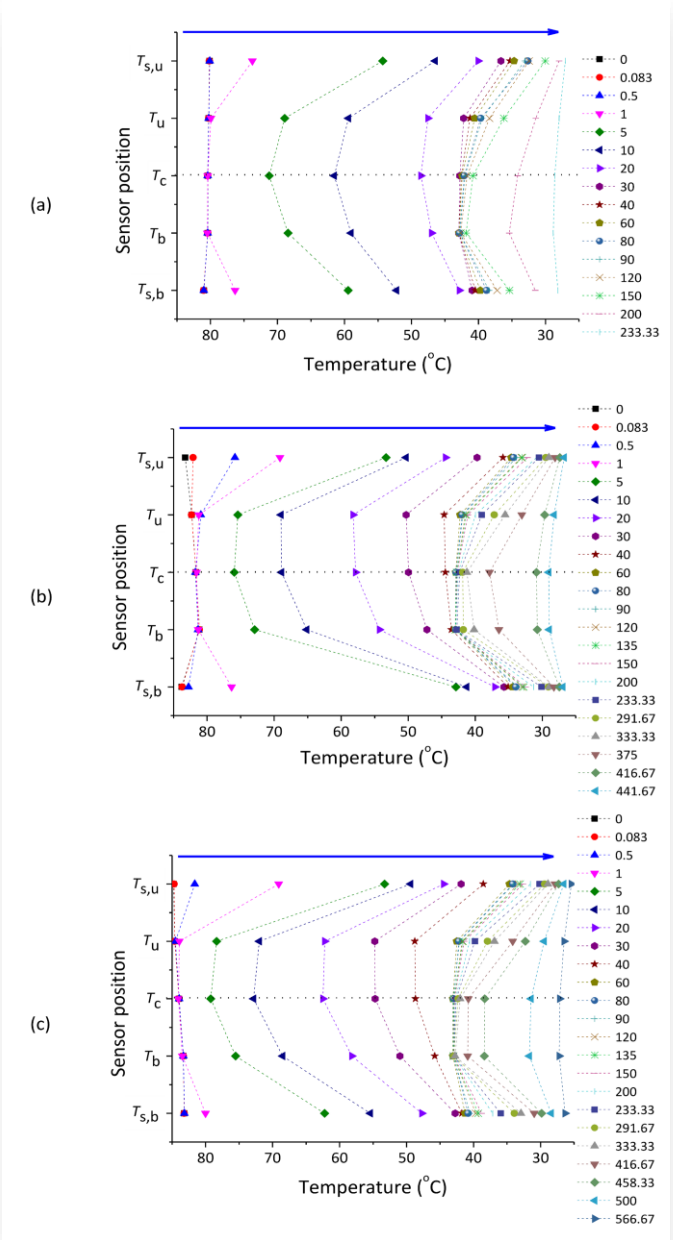

Fig. 7. Temperature distribution along the vertical direction at certain times (in minute) during the solidification of LA in a spherical shell with diameters of (a) 44 mm, (b) 63 mm, and (c) 74 mm.

3.3. Controlling the heat transfer rate of PCM

During the charging and discharging processes of PCM, heat exchange between PCM and its environment occurs at the surface layer of the shell, and is dominated by conduction and convection. The rate of heat conduction through a wall is expressed using Fourier's equation [20] and is proportional to the temperature difference across the wall (ΔT) and the heat transfer area (A) but is inversely proportional to the wall thickness (L)

$$\dot{Q}_{\text{conduction}} = -\kappa_c A \frac{\Delta T}{L}, \tag{1}$$

where κ_c is the thermal conductivity of the container material and is a measure of its ability to conduct heat. Despite the complexity of convection, the rate of convection heat transfer is proportional to the temperature difference, and is conveniently expressed by Newton's law of cooling as follows [20]:

$$\dot{Q}_{\text{convection}} = hA(T_w - T_{\text{PCM}}), \tag{2}$$

where h is the convective heat transfer coefficient, A is the surface area through which the convective heat transfer occurs, T_w is the boundary temperature, and T_{PCM} is the temperature of the PCM. We note that h is not a property of the material, as the thermal conductivity is, because it is dependent on several external factors, such as the properties of the fluid, pressure, and fluid velocity.

The melting and solidification processes of PCM-based TES systems are highly complex and involve conduction and natural convection heat transfer mechanisms with different dominant mechanisms. The power density of the PCM as a TES system can be calculated as:

$$P = \kappa_{\text{PCM}} \frac{dT}{dx} + h(T_{\text{PCM}} - T_a), \tag{3}$$

where κ_{PCM} is the thermal conductivity of PCM and T_a is the ambient temperature.

Focusing on constrained melting, the description of the melting mechanism begins with PCM initially in the solid phase with conductive heat transfer. As time increased at the beginning of the melting process, the liquid phase started to form when the solid–liquid interface was parallel to the heating boundary. In this case, the heat transfer process was still dominated by heat conduction [38,41], and the liquid formation of PCM was relatively constant because of the direct contact between the inner wall and solid PCM [27,41]. As melting progressed, the layer of liquid PCM increased, particularly at the upper part of the shell [27,37–38,41]; thus, the heat conduction was significantly reduced. Hence, a transition stage from dominant heat conduction to heat convection occurred [38], and the shape of the solid–liquid interface was no longer parallel to the heating boundary. Instead, it had an irregular curve shape with a position slightly lower than the centre of the shell owing to the higher density of the solid phase [21,41]. This irregularly shaped phase front was caused by natural convection when the liquid layer thickness increased. In this case, natural convection occurred because the warm liquid PCM rose along the hot wall, whereas the cooler liquid in the centre flowed down to replace the warmer fluid. This phenomenon creates unstable fluid circulation inside the shell, known as 'buoyancy-driven convection' [21,42]. With an increase in the amount of liquid phase, the size of the solid phase decreased before finally reaching a fully melted state.

In the solidification process, the initial condition was a melted PCM with dominant convective heat transfer. As time increased, the temperature of the liquid layer adjacent to the inner wall decreased, and solidification propagated slowly towards the centre of the sphere concentrically, with the solid–liquid interface being relatively parallel to the cool boundary [37,43]. As cooling progressed, the temperature and liquid fraction decreased rapidly, and the buoyancy-driven convection moved the cooler liquid downward owing to its higher density. Under these conditions, the solid–liquid interface was relatively spherically symmetric, with the solid phase being thicker at the bottom of the shell, and a transition from the dominant heat convection stage to the heat conduction transition stage occurred [30,35]. As time increased, the amount of cold-liquid PCM decreased before the PCM reached its full solid state. However, at the end of solidification, the front phase is relatively irregular owing to the formation of voids caused by the shrinkage of the solid PCM [43]. The number, size and distribution of voids are influenced by the initial temperature and liquid viscosity of the PCM, in addition to the ratio of the surface area relative to the volume of the sphere (A/V), because a larger surface area provides a faster cooling rate and makes it easier to trap voids [44].

Following the T-history method [45,46], we considered the time derivative of the PCM temperature to determine the melting and solidification periods. The resulting dT/dt–t graph plotted along the T–t graph is shown in the upper part of Fig. 8. For melting (left), each of the three temperature sensors exhibits two peaks (t_m and t_{pm}) on the derivative curve corresponding to the beginning and end of melting. The melting period Δt_m was determined as the difference between t_m from T_u data and t_{pm} from T_b data. In contrast, for solidification (right), the three temperature sensors showed a constant value of zero in the temperature derivative curve at almost the same time (t_f) owing to the latent heat release, and an inflection point (t_{if}) in the $dT/dt - t$ curve marked the end of the solidification process [47,48]. The solidification period Δt_c is defined as the difference between t_{if} and t_f, with t_{if} obtained from T_u data. The results (bottom part of Fig. 8) show that the melting and solidification periods increased with increasing shell size because of the larger amount of stored heat, which agrees with the results of previous studies [33,49–51].

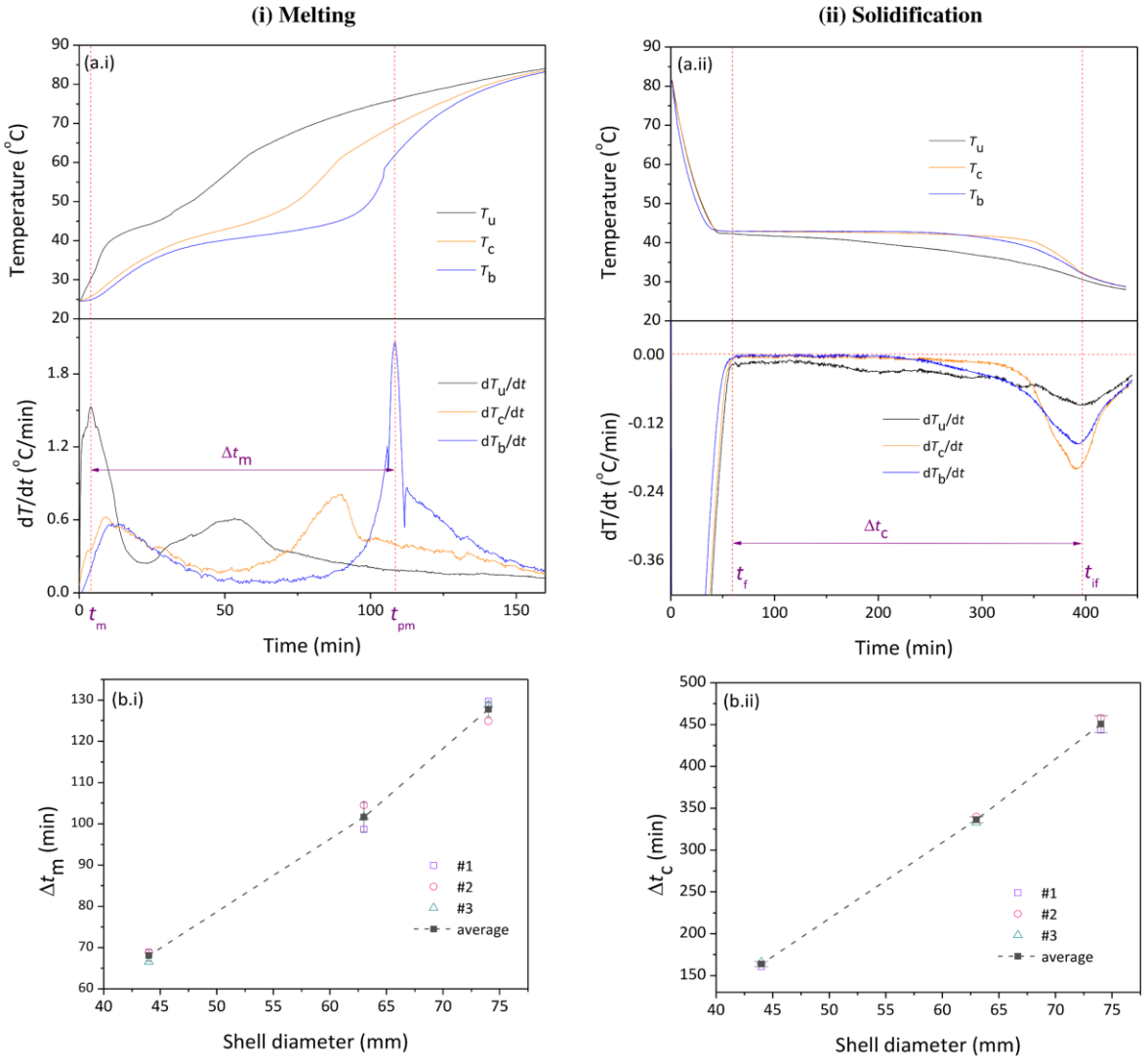

Fig. 8. Time-dependent temperature data of T_u, T_c, and T_b and their time derivatives to determine the melting (left) and solidification (right) periods; and bottom: the melting/solidification periods of LA in a spherical shell with various diameters. For each shell size, we show the data from three repetitive measurements with means and standard deviations.

An asymmetry exists between the behaviours of the melting and solidification processes. In other words, melting and solidification do not simply reverse the process direction. The melting process was dominated by natural convection [27,37,38], whereas the solidification process was dominated by heat conduction [30,37,50]. As shown in bottom of Fig. 8, shorter melting period associated with heat absorption than the solidification period associated with the heat release agrees with the prediction that convection is considerably more efficient than conduction for heat transfer [20]. With convective dominance, the heat transfer rate of the melting process is highly sensitive to the properties of the surrounding fluid, nature of the fluid motion, and bulk fluid velocity.

The optimal performance of PCM for diurnal applications requires a balance between the charging and discharging periods. This can be achieved, for example, by using different heat transfer fluids as media during melting and solidification. From a geometric perspective, for the spherical geometry of the PCM, by decreasing the diameter of the sphere, the *A*/*V* ratio can be increased to enhance the heat transfer [27]. Additionally, various active and passive methods can be used to control the heat transfer rate of PCM [52,53]. Passive methods involve using additives or surface modification techniques to increase the thermal conductivity of PCM or composite PCM. This method is typically performed by adding dopant particles with high thermal conductivity to the PCM [54,55], inserting a metal matrix into the PCM [56], extending the surface using finned tubes with various geometries [57], using porous materials [58], or microencapsulating the PCM [59]. The active method relies on an external field, such as mechanical disturbances, vibrations, ultrasound, electric fields, or magnetic fields [60]. The effectiveness of ultrasound in enhancing heat transfer is closely related to the ultrasonic power and action time [61]. In the case of an electric field, electric body forces, including the Coulomb forces produced by an external electric field, induce flow [62], bubble generation [63,64], or complex compounds [63,65–67] that enhance heat transfer. In contrast, the effect of a magnetic field or its combination with magnetic dopant particles [68–70] controls the convective heat transfer from the PCM and modifies the shape of the solid-liquid interface [71]. The effectiveness of electric and magnetic fields is closely related to the polarisability and magnetisation of the material and its effect on the change in the Gibbs free energy [72,73]. We note that apart from different heat transfer mechanisms, from a thermodynamic point of view, melting is related to an increase in the entropy of the system, whereas solidification is related to a decrease in entropy. These two processes are irreversible to each other [74]. Finally, the asymmetry between melting and solidification may be intricately related to the asymmetry between heating and cooling, as has been recently studied in the thermal kinematics of microscopic systems [75].

4. Conclusions

In this paper, we present the results of an experimental study on the heat exchange of the organic phase change material (PCM) of lauric acid in a spherical shell in an air environment as well as its implications for the heat transfer mode inside the shell and phase change characteristics. From the time-dependent temperature data inside and on the surface of the shell, we found that melting was dominated by convection, whereas solidification was dominated by conduction. The convection intensity increases with increasing shell size. Hence, the melting process depends on the properties of the surrounding fluid, nature of the fluid motion, and bulk fluid velocity. Owing to the relatively high convection transfer rate, latent heat absorption following a solid-to-liquid phase change does not occur at a constant temperature. The sensor at the bottom half of the shell showed a smaller temperature gradient in the latent phase than in the solid and liquid sensible phases. This differs from the solidification process, in which a latent heat release accompanied by a liquid-to-solid phase transition occurs at a relatively constant temperature. In addition, for a given shell size, the melting period was shorter than the solidification period.

Because of the asymmetry between the melting and solidification processes, controlling the heat transfer rate is important for achieving a balance between charging and discharging to optimise the performance of PCM for diurnal applications. From a geometric point of view, this can be achieved by choosing a certain shell diameter, considering that the *A*/*V* ratio increases with a decreasing shell diameter, which enhances the heat transfer. From the heat transfer medium, a fluid with a higher density, such as water, is suitable for solidification while melting in an air environment because of its longer solidification time. In addition, we discuss active and passive methods for controlling heat transfer in PCM. Passive methods rely on the use of dopant particles, metal matrices, and surface modifications, whereas active methods require additional external energy, such as mechanical energy, electrical or magnetic field energy. However, because of the different dominant heat transfer mechanisms for melting and solidification, different strategies may be applied to the two processes. Controlling heat transfer in the charging and discharging processes of PCM is highly beneficial for future PCM technologies, although it is challenging for practical applications.

Acknowledgements

This study presents the output of the P2MI ITB 2024 research scheme. We thank Editage (www.Editage.com) for English language editing.

References

[1] Magendran, S.S., Saleem, F., Khan, A., Mubarak, N.M., & Vaka, M. (2019). Synthesis of organic phase change materials (PCM) for energy storage applications : A review. *Nano-Structures & Nano-Objects*, 20, 100399. doi: 10.1016/j.nanoso.2019.100399

[2] Fleischer, A.S. (2015). *Thermal energy storage using phase change materials: Fundamentals and applications*. Springer Briefs in Applied Sciences and Technology. Springer Cham. doi: 10.1007/978-3-319-20922-7

[3] Sari, A. (2003). Thermal reliability test of some fatty acids as PCMs used for solar thermal latent heat storage applications, *Energy Conversion and Management*, 44(14), 2277–2287. doi: 10.1016/S0196-8904(02)00251-0

[4] Sarı, A., & Kaygusuz, K. (2003). Some fatty acids used for latent heat storage : thermal stability and corrosion of metals with

respect to thermal cycling. *Renewable Energy*, 28, 939–948. doi: 10.1016/S0960-1481(02)00110-6

[5] Majó, M., Sánchez, R., Barcelona, P., García, J., Fernández, A.I., & Barreneche, C. (2021). Degradation of fatty acid phase-change materials (PCM): New approach for its characterization. *Molecules*, 26(4), 1–11. doi: 10.3390/molecules26040982

[6] Kahwaji, S., Johnson, M.B., Kheirabadi, A.C., Groulx, D., & White, M.A. (2017). Fatty acids and related phase change materials for reliable thermal energy storage at moderate temperatures. *Solar Energy Materials and Solar Cells*, 167, 109–120. doi: 10.1016/j.solmat.2017.03.038

[7] Rozanna, D., Chuah, T.G., Salmiah, A., Choong, T.S.Y., & Sa'ari, M. (2005). Fatty Acids as Phase Change Materials (PCMs) for Thermal Energy Storage: A Review. *International Journal of Green Energy*, 1**(**4), 495–513. doi: 10.1081/ge-200038722

[8] Nazari, M., Jebrane, M., & Terziev, N. (2021). Multicomponent bio-based fatty acids system as phase change material for low temperature energy storage. *Journal of Energy Storage*, 39, 10264. doi: 10.1016/j.est.2021.102645

[9] Duquesne, M., Mailhé, C., Doppiu, S., Dauvergne, J.L., Moreno, S.S., Godin, A., Fleury, G., Rouault, F., & del Barrio, E.P. (2021). Characterization of Fatty Acids as Biobased Organic Materials for Latent Heat Storage. *Materials*, 14(16), 4707. doi: 10.3390/ma14164707

[10] Kurdi, A., Almoatham, N., Mirza, M., Ballweg, T., & Alkahlan, B. (2021). Potential phase change materials in building wall construction − a review. *Materials*, 14, 18. doi: 10.3390/ma14185328

[11] Hyun, D.C., Levinson, N.S., Jeong, U., & Xia, Y. (2014). Emerging applications of phase-change materials (PCMs): Teaching an old dog new tricks. *Angewandte Chemie International Edition*, 53(15), 3780–3795. doi: 10.1002/anie.201305201

[12] Zare, M., & Mikkonen, K.S. (2023). Phase Change Materials for Life Science Applications. *Advanced Functional Materials*, 33, 2213455. doi: 10.1002/adfm.202213455

[13] Rathore, P.K.S., & Shukla, S.K. (2019). Potential of macroencapsulated PCM for thermal energy storage in buildings: A comprehensive review. *Construction and Building Materials*, 225, 723–744. doi: 10.1016/j.conbuildmat.2019.07.221

[14] Liu, Z., Teng, R., & Sun, H. (2022). Application of Phase Change Energy Storage in Buildings: Classification of Phase Change Materials and Packaging Methods. *Thermal Science*, 26(5), 4315–4332. doi: 10.2298/TSCI211122045L

[15] Liu, Z., Yu, Z.(J.), Yang, T., Qin, D., Li, S., Zhang, G., Haghighat, F., & Joybari, M.M. (2018). A review on macro-encapsulated phase change material for building envelope applications. *Building and Environment*, 144, 281–294. doi: 10.1016/j.buildenv.2018.08.030

[16] Wonorahardjo, S., Sutjahja, I.M., & Kurnia, D. (2019). Potential of Coconut Oil for Temperature Regulation in Tropical Houses. *Journal of Engineering Physics and Thermophysics*, 92**(**1), 80−88. doi: 10.1007/s10891-019-01909-7

[17] Wonorahardjo, S., Sutjahja, I.M., Damiati, S.A., & Kurnia, D. (2020). Adjustment of indoor temperature using internal thermal mass under different tropical weather conditions. *Science and Technology for the Built Environment*, 26(2), 115–127. doi: 10.1080/23744731.2019.1608126

[18] Wei, J., Kawaguchi, Y., Hirano, S., & Takeuchi, H. (2005). Study on a PCM heat storage system for rapid heat supply. *Applied Thermal Engineering*, 25(17–18), 2903–2920. doi: 10.1016/j.applthermaleng.2005.02.014

[19] Archibold, A.R., Gonzalez-Aguilar, J., Rahman, M.M., Yogi Goswami, D., Romero, M., & Stefanakos, E.K. (2014). The melting process of storage materials with relatively high phase change temperatures in partially filled spherical shells. *Applied Energy*, 116, 243–252. doi: 10.1016/j.apenergy.2013.11.048

[20] Cengel, Y.A. (2002). *Heat Transfer, A Practical Approach*, (2nd ed.). McGraw Hill.

[21] Tan, F.L. (2008). Constrained and unconstrained melting inside a sphere. *International Communications in Heat Mass Transfer*, 35(4), 466–475. doi: 10.1016/j.icheatmasstransfer.2007.09.008

[22] Kothari, R., Revankar, S.T., Sahu, S.K., & Kundalwal, S.I. (2020). A comparative study of constrained and unconstrained melting inside a sphere. *International Conference on Nuclear Engineering Collacated with the ASME 2020 Power Conference*, ICONE 3, V003T12A002. 4-5 August, Virtual conference. doi: 10.1115/ICONE2020-16056.

[23] Goel, V., Dwivedi, A., Kumar, R., Kumar, R., Pandey, A.K., Chopra, K., & Tyagi, V.V. (2023). PCM-assisted energy storage systems for solar-thermal applications: Review of the associated problems and their mitigation strategies. *Journal of Energy Storage*, 69, 107912. doi: 10.1016/j.est.2023.107912

[24] Du, K., Calautit, J., Wang, Z., Wu, Y., & Liu, H. (2018). A review of the applications of phase change materials in cooling, heating and power generation in different temperature ranges. *Applied Energy*, 220, 242–273. doi: 10.1016/j.apenergy.2018.03.005

[25] Rizan, M.Z.M., Tan, F.L., & Tso, C.P. (2012). An experimental study of n-octadecane melting inside a sphere subjected to constant heat rate at surface. *International Communications in Heat Mass Transfer*, 39(10), 1624–1630. doi: 10.1016/j.icheatmasstransfer.2012.08.003

[26] Galione, P.A., Lehmkuhl, O., Rigola, J., & Oliva, A. (2015). Fixed-grid numerical modeling of melting and solidification using variable thermo-physical properties - Application to the melting of n-Octadecane inside a spherical capsule. *International Communications in Heat Mass Transfer*, 86, 721–743. doi: 10.1016/j.ijheatmasstransfer.2015.03.033

[27] Hosseinizadeh, S.F., Rabienataj Darzi, A.A., Tan, F.L., & Khodadadi, J.M. (2013). Unconstrained melting inside a sphere. *International Journal of Thermal Sciences*, 63, 55–64. doi: 10.1016/j.ijthermalsci.2012.07.012

[28] Tan, F.L., Hosseinizadeh, S.F., Khodadadi, J.M., & Fan, L. (2009). Experimental and computational study of constrained melting of phase change materials (PCM) inside a spherical capsule. *International Journal of Heat and Mass Transfer*, 52(15–16), 3464–3472. doi: 10.1016/j.ijheatmasstransfer.2009.02.043

[29] Ismail, K.A.R., & Moraes, R.I.R. (2009). A numerical and experimental investigation of different containers and PCM options for cold storage modular units for domestic applications. *International Journal of Heat and Mass Transfer*, 52, 4195–4202. doi: 10.1016/j.ijheatmasstransfer.2009.04.031

[30] Ettouney, H., El-Dessouky, H., & Al-Ali, A. (2005). Heat transfer during phase change of paraffin wax stored in spherical shells, *Journal of Solar Energy Engineering*, 127**(**3), 357–365. doi: 10.1115/1.1850487

[31] Cofré-Toledo, J., Roa-Cossio, D., Vasco, D.A., Cabeza, L.F., & Rouault, F. (2022). Numerical simulation of the melting and solidification processes of two organic phase change materials in spherical enclosures for cold thermal energy storage applications. *Journal of Energy Storage*, 51, 104337. doi: 10.1016/j.est.2022.104337

[32] Assis, E., Katsman, L., Ziskind, G., & Letan, R. (2007). Numerical and experimental study of melting in a spherical shell. *International Journal of Heat and Mass Transfer*, 50(9–10), 1790–1804. doi: 10.1016/j.ijheatmasstransfer.2006.10.007

[33] Li, W., Li, S.G., Guan, S., Wang, Y., Zhang, X., & Liu, X. (2017). Numerical study on melt fraction during melting of phase change material inside a sphere. *International Journal of Hydrogen Energy*, 42(29), 18232–18239. doi: 10.1016/j.ijhydene.2017.04.136

[34] Ghosh, D., Guha, C., & Ghose, J. (2019). Numerical investigation of paraffin wax solidification in spherical and rectangular cavity. *Heat Mass Transfer*, 55, 3547–3559. doi: 10.1007/s00231-019-02680-4

[35] Nazzi Ehms, J.H., De Césaro Oliveski, R., Oliveira Rocha, L.A., & Biserni, C. (2018). Theoretical and numerical analysis on phase change materials (PCM): A case study of the solidification process of erythritol in spheres. *International Journal of Heat and Mass Transfer*, 119, 523–532. doi: 10.1016/j.ijheatmasstransfer.2017.11.124

[36] Assis, E., Ziskind, G., & Letan, R. (2009). Numerical and experimental study of solidification in a spherical shell. *Journal of Heat and mass Transfer*, 131(2), 024502. doi: 10.1115/1.2993543

[37] Li, W., Wang, Y.H., & Kong, C.C. (2015). Experimental study on melting/solidification and thermal conductivity enhancement of phase change material inside a sphere. *International Communications in Heat Mass Transfer*, 68, 276–282. doi: 10.1016/j.icheatmasstransfer.2015.09.004

[38] Prabakaran, R., Kumar, J.P.N., Mohan Lal, D., Selvam, C., & Harish, S. (2020). Constrained melting of graphene-based phase change nanocomposites inside a sphere. *Journal of Thermal Analysis and Calorimetry*, 139(2), 941–952. doi: 10.1007/s10973-019-08458-4

[39] Sutjahja, I.M., Anggraini, Y., & Yusuf, A. (2024). Acceleration of Heat Discharge of Composite Lauric Acid Using Magnetic Dopant. *Journal of Energy Storage*, 86, 111219. doi: 10.1016/j.est.2024.111219

[40] Shokouhmand, H., & Kamkari, B. (2013). Experimental investigation on melting heat transfer characteristics of lauric acid in a rectangular thermal storage unit. *Experimental Thermal and Fluid Science*, 50, 201–212. doi: 10.1016/j.expthermflusci.2013.06.010

[41] Sattari, H., Mohebbi, A., Afsahi, M.M., & Yancheshme, A.A. (2017). CFD simulation of melting process of phase change materials (PCMs) in a spherical capsule. *International Journal of Refrigeration*, 73, 209–218. doi: 10.1016/j.ijrefrig.2016.09.007

[42] Khodadadi, J.M., & Zhang, Y. (2001). Effects of buoyancy-driven convection on melting within spherical containers. *International Journal of Heat and Mass Transfer*, 44(8), 1605–1618. doi: 10.1016/S0017-9310(00)00192-7

[43] Chan, C.W., & Tan, F.L. (2006). Solidification inside a sphere - An experimental study. *International Communications in Heat Mass Transfer*, 33(3), 335–341. doi: 10.1016/j.icheatmasstransfer.2005.10.010

[44] Revankar, S.T., & Croy, T. (2007). Visualization study of the shrinkage void distribution in thermal energy storage capsules of different geometry. *Experimental Thermal and Fluid Science*, 31(3), 181–189. doi: 10.1016/j.expthermflusci.2006.03.026

[45] Peck, J.H., Kim, J.J., Kang, C., & Hong, H. (2006). A study of accurate latent heat measurement for a PCM with a low melting temperature using T-history method. *International Journal of Refrigeration*, 29(7), 1225–1232. doi: 10.1016/j.ijrefrig.2005.12.014

[46] Yinping, Z., & Yi, J. (1999). A simple method, the T-history method, of determining the heat of fusion, specific heat and thermal conductivity of phase-change materials. *Measurement Science and Technology*, 10(3), 201–205. doi: 10.1088/0957-0233/10/3/015

[47] Hong, H., Kim, S.K., & Kim, Y.S. (2004). Accuracy improvement of T-history method for measuring heat of fusion of various materials. *International Journal of Refrigeration*, 27, 360–366. doi: 10.1016/j.ijrefrig.2003.12.006

[48] Sutjahja, I.M., Silalahi, A., Kurnia, D., & Wonorahardjo, S. (2018). Thermophysical parameters and enthalpy-temperature curve of phase change material with supercooling from T-history data. *UPB Scientific Bulletin, Series B: Chemistry and Materials Science*, 80(2), 57–70.

[49] Lago, T.G.S., Ismail, K.A.R., Lino, F.A.M., & Arabkoohsar, A. (2020). Experimental correlations for the solidification and fusion times of PCM encapsulated in spherical shells. *Experimental Heat Transfer*, 33(5), 440–454. doi: 10.1080/08916152.2019.1656301

[50] Ismail, K.A.R., & Moraes, R.I.R. (2009). A numerical and experimental investigation of different containers and PCM options for cold storage modular units for domestic applications. *International Journal of Heat and Mass Transfer*, 52, 19–20, 4195–4202. doi: 10.1016/j.ijheatmasstransfer.2009.04.031

[51] Chandrasekaran, P., Cheralathan, M., & Velraj, R. (2015). Influence of the size of spherical capsule on solidification characteristics of DI (deionized water) water for a cool thermal energy storage system – An experimental study. *Energy*, 90, 807–813. doi: 10.1016/j.energy.2015.07.113

[52] Diaconu, B.M., Cruceru, M., & Anghelescu, L. (2023). A critical review on heat transfer enhancement techniques in latent heat storage systems based on phase change materials. Passive and active techniques, system designs and optimization, *Journal of Energy Storage*, 61, 106830. doi: 10.1016/j.est.2023.106830

[53] Jegadheeswaran, S., Sundaramahalingam, A.,, &, Pohekar, S.D. (2021). Alternative Heat Transfer Enhancement Techniques for Latent Heat Thermal Energy Storage System: A Review. *International Journal of Thermophysics*, 42, 171. doi: 10.1007/s10765-021-02921-x

[54] Sutjahja, I.M., Silalahi, A.O., Wonorahardjo, S., & Kurnia, D. (2019). Thermal conductivity of phase-change material $CACL_2{\cdot}6H_2O$ with ZnO nanoparticle dopant based on temperature-history method. *Revista Romana de Materiale / Romanian Journal of Materials*, 49(2), 185–192.

[55] Sutjahja, I.M., Silalahi, A.O., Kurnia, D., & Wonorahardjo S. (2019). The role of particle dopant to the thermal conductivities of PCM coconut oil by means of the T-history method. *Journal of Physics: Conference Series*, 1204, 012056. *The 7th Asian Physics Symposium*, 29-31 August 2017, Bandung, Indonesian. doi:10.1088/1742-6596/1204/1/012056

[56] Jourabian, M., Farhadi, M., & Rabienataj Darzi, A.A. (2016). Heat transfer enhancement of PCM melting in 2D horizontal elliptical tube using metallic porous matrix. *Theoretical and Computational Fluid Dynamics*, 30, 579–603. doi: 10.1007/s00162-016-0402-0

[57] Sayehvand, H.-O., Abolfathi, S., & Keshavarzian, B. (2023). Investigating heat transfer enhancement for PCM melting in a novel multi-tube heat exchanger with external fins. *Journal of Energy Storage*, 72, 108702. doi: 10.1016/j.est.2023.108702

[58] Zhao, C.Y., Zhou, D., & Wu, Z.G. (2011). Heat transfer of phase change materials (PCMs) in porous materials. *Frontiers in Energy*, 5, 174–180. doi: 10.1007/s11708-011-0140-3

[59] Rostami, J. (2021). Convective heat transfer by micro-encapsulated PCM in a mini-duct. *International Journal of Thermal Sciences*, 161, 106737. doi: 10.1016/j.ijthermalsci.2020.106737

[60] Wu, Y., Zhang, X., Xu, X., Lin, X., & Liu, L. (2020). A review on the effect of external fields on solidification, melting and heat transfer enhancement of phase change materials, *Journal of Energy Storage*, 31, 101567. doi: 10.1016/j.est.2020.101567

[61] Zhang, N., & Du, Y. (2018). Ultrasonic enhancement on heat transfer of palmitic-stearic acid as PCM in unit by experimental study. *Sustainable Cities and Society*, 43, 532–537. doi: 10.1016/j.scs.2018.08.040

[62] Sun, Z., Zhang, Y., Luo, K., Pérez, A.T., Yi, H., & Wu, J. (2022). Experimental investigation on melting heat transfer of an organic material under electric field. *Experimental Thermal and Fluid Science*, 131, 110530. doi: 10.1016/j.expthermflusci.2021.110530

[63] Shahriari, A., Acharya, P.V., Carpenter, K., & Bahadur, V. (2017). Metal-Foam-Based Ultrafast Electronucleation of Hydrates at Low Voltages. *Langmuir*, 33(23), 5652–5656. doi: 10.1021/acs.langmuir.7b00913

[64] Carpenter, K., & Bahadur, V. (2016). Electronucleation for Rapid and Controlled Formation of Hydrates. *Journal of Physical Chemistry Letters*, 7(13), 2465–2469. doi: 10.1021/acs.jpclett.6b01166

[65] Sutjahja, I.M., Rahman, A., Putri, R.A., Swandi, A., Anggraini, R., Wonorahardjo, S., Kurnia, D., & Wonorahardjo, S. (2019). Electrofreezing of the phase-change material $CaCl_2 \cdot 6H_2O$ and its impact on supercooling and the nucleation time. *Hemijska Industrija*, 73, 363–374. doi: 10.2298/ HEMIND190803034S

[66] Putri, R.A., Yusuf, A., Rahman, A., Anggraini, Y., Kurnia, D., Wonorahardjo, S., Wonorahardjo, S., & Sutjahja, I.M. (2021). Reduction of the supercooling of $Ca(NO_3)_2 \bullet 4H_2O$ using electric field and nucleating agent effects. *Journal of Energy Storage*, 42, 103020. doi: 10.1016/j.est.2021.103020

[67] Swandi, A., Rahman, A., Putri, R.A., Anggraini, R., Kurnia, D., Wonorahardjo, S., & Sutjahja, I.M. (2021). Effect of copper electrode geometry on electrofreezing of the phase-change material CaCl2·6H2O. *Journal of Non-Equilibrium Thermodynamics*, 46(2), 163-174. doi: 10.1515/jnet-2020-0066

[68] Anggraini, Y., Yusuf, A., Viridi, S., Kurnia, D., Wonorahardjo, S., & Sutjahja, I.M. (2024). Magnetic Dopant and Field Effects on the Heat Discharge of Organic PCM based Lauric Acid. *Experimental Thermal and Fluid Science*, 152, 111105. doi: 10.1016/j.expthermflusci.2023.111105

[69] Sheikholeslami, M., & Mahian, O. (2019). Enhancement of PCM solidification using inorganic nanoparticles and an external magnetic field with application in energy storage systems. *Journal of Cleaner Production*, 215, 963–977. doi: 10.1016/j.jclepro.2019.01.122

[70] Zandie, M., Moghaddas, A., Kazemi, A., Ahmadi, M., Feshkache, H.N., Ahmadie, M.H., & Shafripur, M. (2022). The impact of employing a magnetic field as well as Fe_3O_4 nanoparticles on the performance of phase change materials. *Engineering Applications of Computational Fluid Mechanics*, 16(1), 196–214. doi: 10.1080/19942060.2021.2006092

[71] Haddad, Z., Iachachene, F., Zidouni, F., & Oztop, H.F. (2022). Magnetic field effects on melting and solidification of PCMs in an isosceles triangular cavity. *Journal of Thermal Analysis and Calorimetry*, 147, 4697–4709. doi: 10.1007/s10973-021-10857-5

[72] Yusuf, A., Putri, R.A., Rahman, A., Anggraini, Y., Kurnia, D., Wonorahardjo, S., & Sutjahja, I.M. (2021). Time-Controlling the Latent Heat Release of Fatty Acids using Static Electric Field. *Journal of Energy Storage*, 33, 102045. doi: 10.1016/j.est.2020.102045

[73] Rahman, A., Yusuf, A., Putri, R.A., Anggraini, Y., Pujaningsih, F.B., Kurnia, D., Wonorahardjo, S., & Sutjahja, I.M. (2021). Effect of static magnetic field on nucleation of cobalt nitrate hexahydrate. *Materials Research*, 24(6), e20210088. doi: 10.1590/1980-5373-MR-2021-0088

[74] Zemansky, M.W., & Dittman, R.H. (1997). *Heat and Thermodynamics*. McGraw-Hill.

[75] Ibáñez, M., Dieball, C., Lasanta, A., Godec, A., & Rica, R.A. (2024). Heating and cooling are fundamentally asymmetric and evolve along distinct pathways. *Nature Physics*, 20(1), 135–141. doi: 10.1038/s41567-023-02269-z